JOURNAL OF APPLIED ELECTROCHEMISTRY **29**: 185–190, 1999.

Surface shear stress for a submerged jet impingement using electrochemical technique

S. YAPICI, S. KUSLU, C. OZMETIN, H. ERSAHAN, T. PEKDEMIR

Ataturk Universitesi, Mühendislik Fakultesi, Kimya Muhendisligi Bulumu, 25240 Erzurum, Turkey

Received 25 March 1997; accepted in revised form 28 April 1998

The surface local shear stress values were measured for a round submerged jet, with a fully developed turbulent velocity profile, impinging on a flat surface, using the electrochemical limiting current technique with the electrolyte consisting of potassium ferri- and ferrocyanide supported by aqueous sodium hydroxide. Experimental parameters were in the Reynolds number range 9200–73 500, and in the nozzle-to-plate distance range 2–10. The measurements of local shear stress values on the impingement surface in the radial direction were taken, and the effect of the experimental parameters on the behaviour of the shear stress values was discussed.

Keywords: *heat/mass transfer*, *impinging jet*, *limiting current technique*, *shear stress*, *turbulent jets*

List of symbols

A active electrode surface (m^2)
C_f dimensionless wall shear stress
c_∞ bulk concentration of reacting species ($mol\,m^{-3}$)
c_s surface concentration of reacting species ($mol\,m^{-3}$)
D diffusion coefficient ($m^2\,s^{-1}$)
d nozzle diameter, diameter of circular local electrode (m)
h distance from nozzle exit to impingement surface (m)
k' mass transfer coefficient to local electrode ($m\,s^{-1}$)
r radial distance of surface outward from stagnation point (m)
Re Reynolds number ($du_m\rho/\mu$)
S velocity gradient (s^{-1})
u_m average fluid velocity in the nozzle ($m\,s^{-1}$)
u local velocity ($m\,s^{-1}$)
z height from impingement surface (m)
μ viscosity of solution ($N\,s\,m^{-2}$)
ρ density of solution ($kg\,m^{-3}$)
τ_w surface shear stress ($N\,m^{-2}$)

1. Introduction

The use of a single impinging jet, or an array of such jets, as a method of obtaining highly effective surface convective transfer rates has a wide range of industrial and technological applications. Such impinging flow devices allow short flow paths on the surface and therefore have high convective transfer rates. The applications include annealing of metal and plastic sheets, tempering of glass plates, drying of textile, paper, veneer and film materials, cooling of heated components in turbine engines, and deicing of aircraft systems [1, 2]. Impinging jet flows can be classified into groups according to their general characteristics such as shape of the nozzle, the orientation of the jet with respect to the impingement surface etc. Pekdemir [3] classifies according to (i) *fluid types*, submerged and free jets, (ii) *orientation*, oblique and normal jets, (iii) *nozzle shape*, round, slot and elliptic jets, (iv) *impingement surface*, flat and treated surfaces, (v) *the restriction imposed upon the jet at the jet exit*, confined, partially confined and unconfined jets, and (vi) *number of jets*, single and multiple jets. The flow area in a jet flow impinging on a surface is commonly divided into three as shown in Fig. 1: the free jet region, the impingement region and the wall jet region [1].

A considerable amount of investigation has been carried out on the behaviour of impinging jets, especially concentrated on flow and heat transfer characteristics. Donaldsan and Snedeker [4] carried out a study on mean properties of free and impinging jets. Donaldsan *et al.* [5] reported further work on free jet turbulent structure and impingement heat transfer. Turbulent flow characteristics of an impinging jet were studied by Rusell and Hatton [6]. Foss [7] made some measurements of mean flow characteristics for the oblique impingement of an axisymmetric jet and including surface isobar contours and turbulence intensity at different levels over the surface. Lamont and Hunt [8] made detailed measurements of the impingement of underexpanded axisymmetric jets on perpendicular and inclined flat plates by means of surface pressure measurements and shadograph pictures. They reported that the flow structure is extremely complex due to the local flow structure of the jet, and recorded higher maximum pressure on an inclined flat plate than that on a

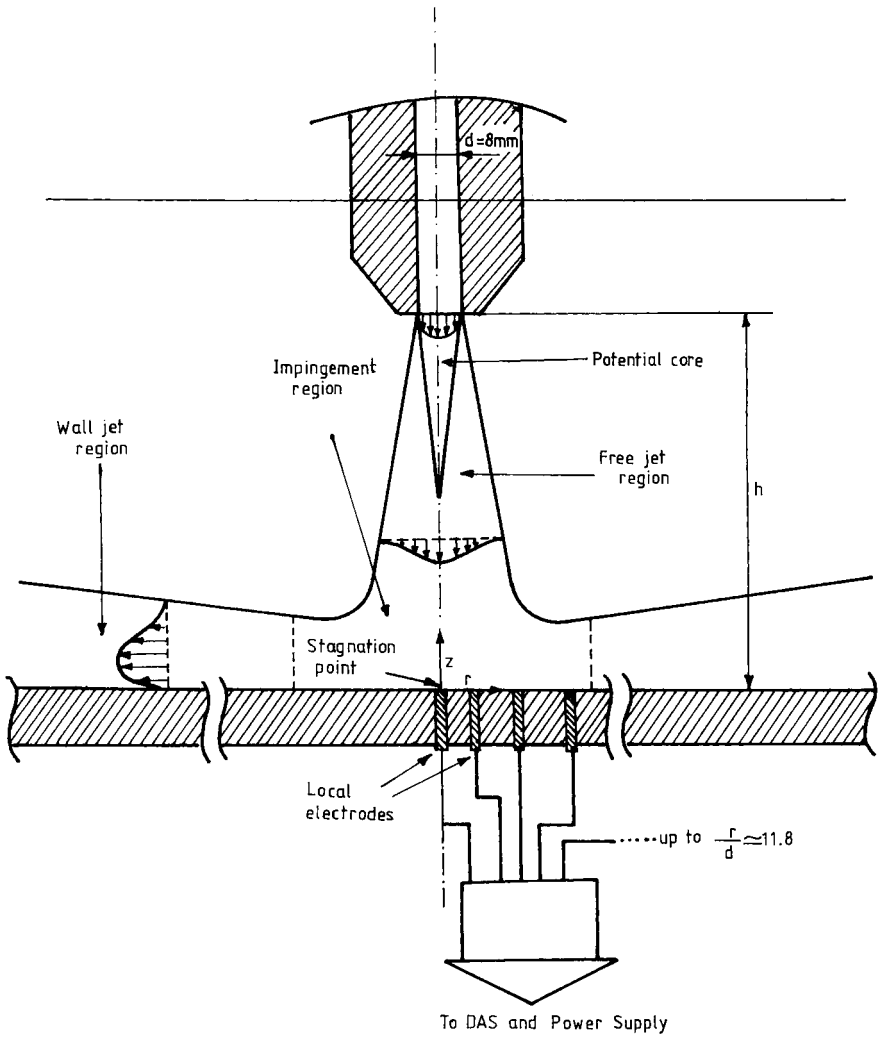

Fig. 1. Impinging jet and flow regions.

perpendicular plate. Deshpande and Vaishnav [9] made flow structure and surface shear stress measurements on a submerged laminar jet impingement on a plane and found that an increase in the height of nozzle exit from the target plane decreases the wall shear stress and a change from parabolic exit velocity to the flat profiles leads to a decrease in wall shear stress due to decreased momentum flux. In addition the structure of an underexpanded round air jet submerged in water [10], measurements of flow in the radial layer of impinging free-surface liquid jets [11], and impinging jet studies for turbulence model assessments [12] can be given as examples of hydrodynamic studies of impinging jets. Mujumdar *et al.* [13], Jambunatham *et al.* [14] and Martin [1] reported good reviews for heat transfer studies for jet impingement.

There are several studies of mass transfer between a plate and an impinging jet using the electrochemical limiting current technique. Kataoka and Mizushina [15] worked on the effect of free stream turbulence on the local rate of mass transfer in an impinging round jet. They observed that the rate of mass transfer for large Schmidt numbers was much more enhanced by the amplified turbulence of free stream than skin friction in the impingement region. It was also determined that the skin friction was almost insensitive to free stream turbulence. Patrick *et al.* [16] and Vallis *et al.* [17, 18] carried out studies on radial distribution of local mass transfer and wall fluxes in an axisymmetric turbulent impinging jet also by the electrochemical technique. They found that Sherwood numbers increased with increasing h/d and converged after a radial distance of $r/d = 8$. They calculated shear stress numerically and compared with experimental data values beyond $r/h = 4$, and found that shear stress reached a maximum at $z/d = 11$ for $Re = 5520$ and at $z/d = 2.2$ for $Re = 20\,682$. Chin and Tsang [19] performed work on mass transfer to circular disc electrodes located in the stagnation region of an impinging jet. They found that the electrode possesses a property of uniform accessibility to the diffusion species if the electrode radius was less than one nozzle diameter for a turbulent jet and half a nozzle diameter for a laminar jet within this region. Alkire and Chen [20] employed single unsubmerged circular jets with the aim of high-speed selective electroplating. Sonin [21] presented a study of mass transfer rates in jet impingement system for electrochemical processes requiring high transfer rates, using

manifold pipes on which orifices were drilled as jets. Nanzer *et al.* [22] investigated the overall mass transfer between submerged circular multijets of electrolyte and flat circular electrodes normal to the jets. They found that overall mass transfer was almost independent of the electrode size; but beyond the impingiment region, there was a pronounced decrease of mass transfer coefficients.

No detailed study on wall shear stress measurements for a submerged impinging jet having a fully developed turbulent velocity profile in the nozzle using the electrochemical technique is known to the authors. The aim of the present study is to measure the surface shear stress of a single round jet impinging on a flat surface.

2. Experimental technique

A schematic diagram of the test section of the experimental rig is given in Fig. 1. For the mass transfer measurements the electrochemical limiting diffusion current technique was used [23, 24]. All the piping system was constructed of PVC to ensure chemical inertness and to avoid the adverse effect of light on the electrochemical solution. In the construction of jet nozzle and flat plate PTFE rod and Acrylic plate were used, respectively. The nozzle was 8 mm i.d. and was designed to give fully developed turbulent flow at the nozzle exit. The test section was equipped with 36 Ni electrodes of 1 mm diameter in three rows at 90° to each other, 12 electrodes in each row, flush with the plate surface at certain intervals beginning from the centre to a distance of $h/d = 11.8$. Only one row was used for the measurements. Since the jet impingement was symmetrical, the measurements from one array from the centre to a certain distance in the radial direction was enough to resemble the system. For the experiments, seven flow rates were employed in the Reynolds number range 9200 to 73 500 based on the nozzle diameter and the average flow velocity in the nozzle, and five nozzle to plate distance values were used, in the range from 2 to 10.

The electrode/electrolyte system used was the potassium ferri-ferrocyanide couple supported with aqueous sodium hydroxide solution. Ni wires of 1 mm diameter were employed as anode and cathode. Only one electrode was used as cathode while all the others were used as anode, that is, a 35 times larger anode area than that of the cathode, to ensure a cathodic controlled process. The physical properties of the electrolyte solution, which consisted of 0.5 M sodium hydroxide 0.01 M potassium ferri- and 0.02 M potassium ferrocyanide, are $\rho = 1027.23\,\mathrm{kg\,m^{-3}}$, $\mu = 1.123\,\mathrm{N\,s\,m^{-2}}$, and $D_{\mathrm{ferri}} = 6.455 \times 10^{-10}\,\mathrm{m^2\,s^{-1}}$, at 20 °C [25]. The test fluid temperature was maintained constant at 20 °C, within ± 1 °C , using a glass coil immersed in the electrolyte reservoir. For the limiting current measurements, the necessary preparatory steps were performed to obtain the most accurate possible measurements, as reviewed by Berger and Ziai [26]. In the experimentation a stable d.c. power supply and a computer controlled data acquisition system were employed.

3. Results and discussions

The mass transfer flux is related to the limiting current as follows:

$$N_{\mathrm{A}} = \frac{I_{\mathrm{lim}}}{nFA} \tag{1}$$

Mass flux can also be expressed in terms of mass transfer coefficient as follows:

$$N_{\mathrm{A}} = k'(c_\infty - c_{\mathrm{S}}) \tag{2}$$

For limiting current conditions, the concentration of reacting species at the cathode, $c_{\mathrm{S}} = 0$, and from Equations 1 and 2, an expression relating mass transfer coefficient directly to the limiting current can be written as

$$k' = \frac{I_{\mathrm{lim}}}{nFc_\infty A} \tag{3}$$

Hanratty [27] showed that the mass transfer coefficients to a finite circular local electrode is related to wall velocity gradient as follows:

$$\frac{k'd}{D} = 0.862\left(S\frac{d^2}{D}\right)^{1/3} \tag{4}$$

where $S = \partial u/\partial z$. The wall shear stress values were calculated using the following expression

$$\tau_{\mathrm{w}} = \mu\frac{\partial u}{\partial z} \tag{5}$$

The shear stress value can be expressed in dimensionless form as

$$C_{\mathrm{f}} = \frac{\tau_{\mathrm{w}}}{0.5\,S\,u_{\mathrm{m}}^2} \tag{6}$$

where u_{m} is the average velocity in the nozzle. The variation of local dimensionless shear stress values with radial distance from the stagnation point to $r/d = 8$ at various Reynolds numbers are shown in Figs 2 and 3. The local shear stresses at the stagnation point, $r/d = 0$, are expected to be zero [28]. Deviation of shear stresses at the stagnation point from zero can be explained by the fact that even if the shear stress in the very stagnation point is zero, for the electric current measured by a circular electrode in the stagnation point it approximates [29] to

$$I_{\mathrm{lim}} \approx \frac{I_0}{\Gamma(4/3)}\left(\frac{B_0}{6}\right)^{1/3} \tag{7}$$

where $I_0 = nFc_\infty D \quad f(Re, Sc)$ is a representative current density and B_0 is a hydrodynamical parameter, and $\Gamma(4/3)$ is a gamma function. The fact that the area of the local electrode is not infinitely small can also result in an average over the surface area from the electrode at the stagnation point. For these reasons, it can be said that the measured shear stress distribution for $r/d < 4$ approximates the real shear stress distribution. The shear stress gave a peak at a distance about $r/d = 1$ for h/d of 2 to 6 and at a distance between approximately 1.5 and 2.5 for h/d of

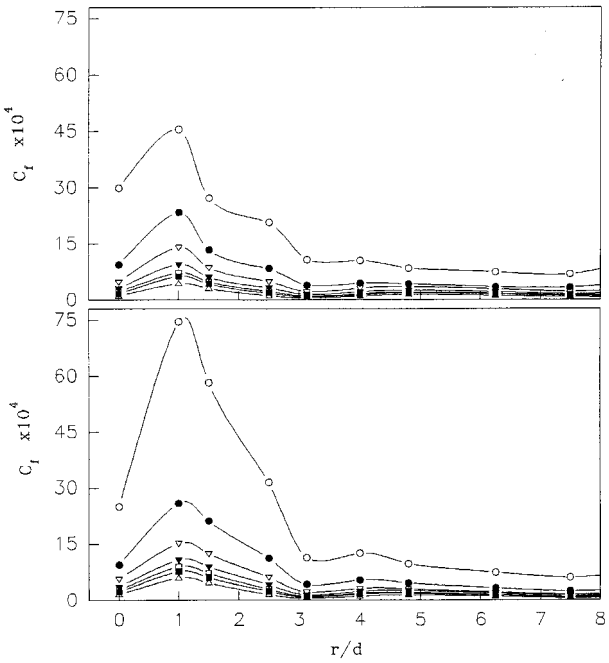

Fig. 2. Behaviour of dimensionless surface shear stress with radial distance for $h/d = 2$ (upper) and 4 (lower). *Re*: (○) 9200, (●) 16 400, (▽) 27 600, (▼) 36 800, (□) 46 000, (■) 55 100 and (△) 73 500.

8 and 10. The width of the peaks were almost the same for $h/d = 2$ and 4, narrower for $h/d = 6$ and larger for $h/d = 8$ and 10. This behaviour can be explained by the development of jet flow and the effect of potential core. For h/d values of 2 and 4 the widths of the potential core are closer, resulting in peaks having almost the same width. With increase in nozzle-to-plate distance, since the thickness of potential core is narrower, a narrower peak is obtained as for $h/d = 6$. The broadening peaks for $h/d = 8$ and 10 can be attributed to the developing jet flow beyond the potential core. While for h/d of 2 to 6 the radial distance of peaks remained constant, the distance shifted from a radial distance of 2.5 to 1.5, getting closer to the stagnation point with increasing *Re* for $h/d = 8$ and 10. The highest peak was obtained for the dimensionless nozzle to the impingement distance of $h/d = 4$ not for $h/d = 2$, and the height of the peak diminished with increasing h/d. This behaviour can be explained by the closer nozzle position to the plate effecting the development of the impingement region. As Reynolds number increased all the nondimensional shear stress values decreased, and showed a tendency to merge. This behaviour is in accord with the findings of Deshpande and Vaishnav [9] and Vallis *et al.* [17], in which the hydrodynamics of a submerged impinging jet in Reynolds number ranges between 1000–2000, and 5500–20 700, respectively, were studied.

The dimensionless shear stress values for different dimensionless distances of the jet exit to the surface at a given Reynolds number are given in Fig. 4 for $Re = 9200$ and 73 500, respectively. The change in width of the peaks can be seen more clearly in this figure. With increase in h/d, the width of the peak decreased up to a distance of $h/d = 6$ and then increased with increasing h/d. This change can be explained by the development of jet flow shown in Fig. 1. The distance of $h/d = 1$–6 lies in the potential core. As plate-to-jet diameter distance increased the narrower part of the potential core effected the plate surface and caused the narrowing peak of dimen-

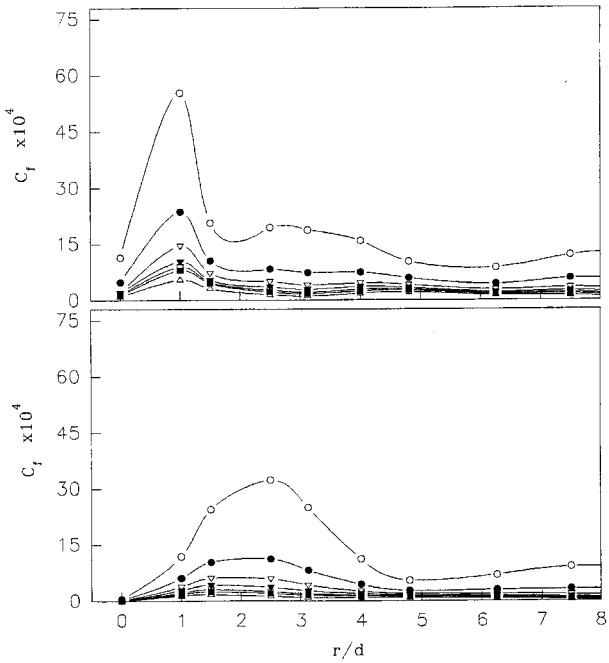

Fig. 3. Behaviour of dimensionless surface shear stress with radial distance for $h/d = 6$ (upper) and 10 (lower). *Re*: (○) 9200, (●) 16 400, (▽) 27 600, (▼) 36 800, (□) 46 000, (■) 55 100 and (△) 73 500.

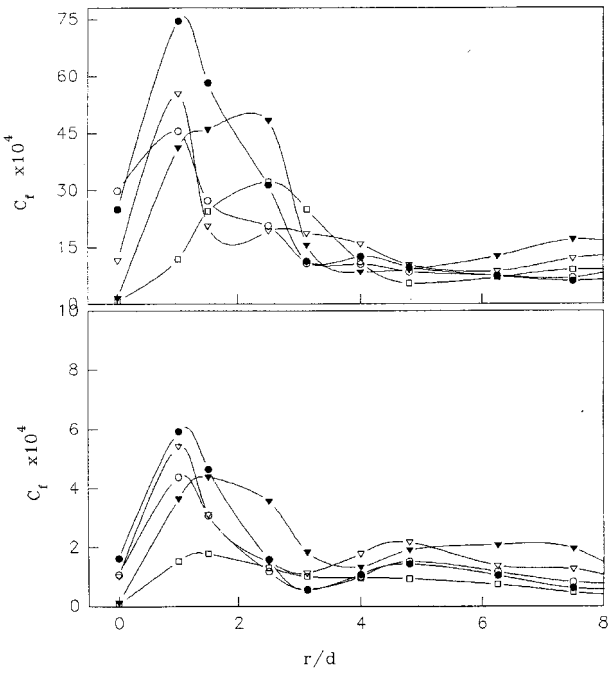

Fig. 4. Behaviour of surface shear stress with dimensionless radial distance for $Re = 9190$ (upper) and 73 500 (lower). h/d: (○) 2, (●) 4, (▽) 6, (▼) 8 and (□) 10.

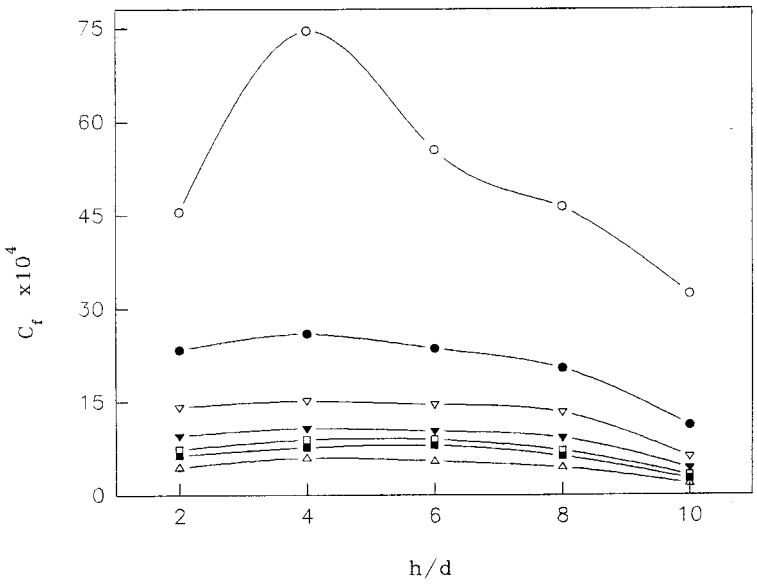

Fig. 5. Variation of dimensionless peak surface shear stress with h/d for different Reynolds number, Re: (○) 9200, (●) 16 400, (▽) 27 600, (▼) 36 800, (□) 46 000, (■) 55 100 and (△) 73 500.

sionless shear stress with increasing nozzle to plate distance up to $h/d = 6$. The narrowest peak for $h/d = 6$ probably coincided with the tip of the potential core. After this distance the developing jet velocity profile gave bigger peaks with increasing h/d. As also seen from this figure, the peak value was the highest for $h/d = 4$, and showed a general tendency to decrease with increasing h/d. Beyond the dimensionless radial distance of $r/d = 4$, it is difficult to make any clear interpretation to explain the difference in behaviour between the results for the same Reynolds number at different h/d values, but it is possible to say that the dimensionless shear stress values showed a tendency to converge to a single value after r/d of about 4; this can be attributed to the occurrence of transition from an accelerating stagnation region flow to a decelerating wall jet region at about $r/d = 4$. Similar behaviour was observed by Rao and Trass

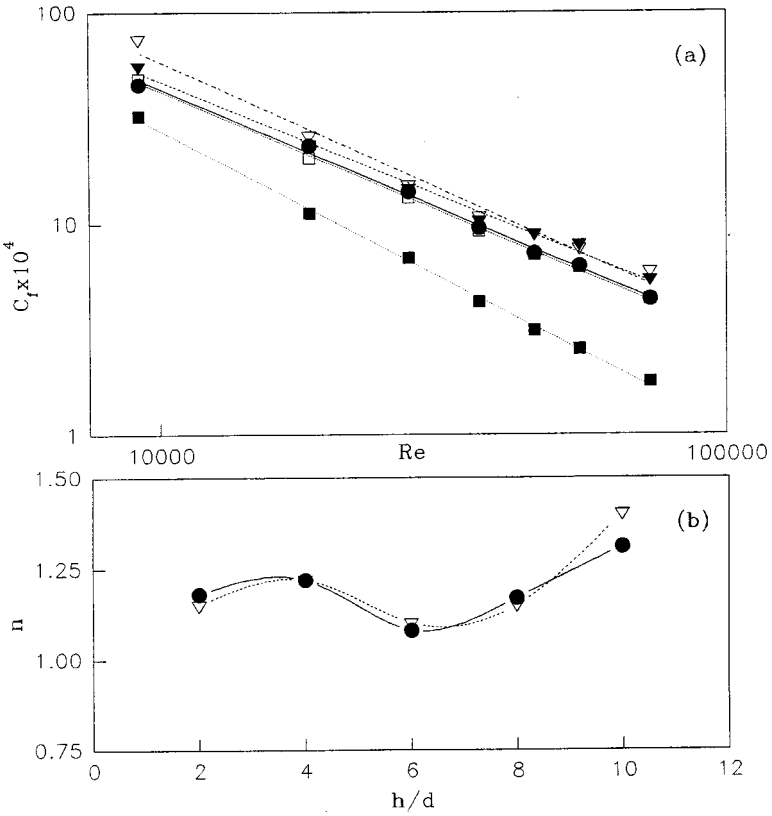

Fig. 6. (a) Correlations of dimensionless peak shear stress values with Reynolds number. Key for h/d: (●) 2, (▽) 4, (▼) 6, (□) 8 and (■) 10. (b) Comparison of Reynolds numbers power for peak values and average values over $r/d = 11.8$. Key: (●) average and (▽) peak.

[30]. They determined that the local mass transfer coefficient was independent of nozzle-to-plate spacing at radial positions grater than 4.5 nozzle diameters from the stagnation point. The shear stress values do not exhibit a regular behaviour after this point; however, no significiant change occurs.

The peak values of the dimensionless shear stress against the dimensionless distance of nozzle exit to impingement surface are given in Fig. 5 for various Reynolds numbers. The correlations were searched to see the relation between Reynolds number and the peak shear stress values, and the average shear stress values obtained by averaging the local values over the radial distance-to-nozzle diameter from stagnation point to $r/d = 11.8$; the correlation for the peak values is presented graphically in Fig. 6(a). Regression analysis in the form

$$C_f \propto 1/Re^n \tag{8}$$

gave an indication of the Reynolds number dependence . The power on the Reynolds number, n, had a value between 1.10 and 1.40 for the maximum dimensionless shear stress values, and between 1.08 and 1.31 for the averaged values. For the same h/d value, the Reynolds number power are very close for the peak and the averaged values, with a maximum deviation of 6%. The change in Reynolds number power with h/d is shown in Fig. 6(b).

4. Conclusions

The results showed that the nondimensional local shear stresses values decreased with increasing Reynolds number and had a tendency to converge at higher Reynolds numbers. The shear stress values gave a peak at a distance about $r/d = 1$ for h/d of 2 to 6 and at a distance between 1.5 and 2.5 for h/d of 8 and 10. While the radial position of the peaks remained constant and the width of the peaks were narrower for h/d of 2 to 6, it shifted from a radial distance of 2.5 to 1.5 towards the stagnation point with increase in Reynolds number, and the width of the peaks increased for $h/d = 8$ and 10. The highest peak was obtained for the dimensionless nozzle to impingement surface of 4 and the height of the peak reduced with increasing h/d. when the data correlated in the form ($C_f \propto 1/Re^n$), the correlation of the shear stresses values with Reynolds number showed that the power on the Reynolds number, n, had a value between 1.10 and 1.40 for the peak shear stress values, and between 1.08 and 1.31 for the averaged values.

References

[1] H. Martin, *in* 'Advances in Heat Transfer', edited by J.P. Hartnett and T.F. Irvine, Jr. **13** (1977) 1.
[2] F. P. Incropera and D. P. de Witt, 'Fundamentals of Heat and Mass Transfer', 3rd. edn, J. Wiley & Sons, New York, (1990), p. 431.
[3] T. Pekdemir, 'Convective Mass Transfer from Stationary and Rotating Cylinders in Jet Flow', Ph.D. Thesis, University of Exeter, UK. (1994), p. 24.
[4] C. D. Donaldsan and R. S. Snedeker, *J. Fluid Mechanics* **45** (1971) 281.
[5] C. D. Donaldsan, R. S. Snedeker and D. P. Margolis, *J. Fluid Mechanics* **45** (1971) 477.
[6] P. J. Rusell and P. Hutton, *Proc. Inst. Mech. Eng.* **186** (1972) 52.
[7] J. F. Fos and S. J. Kleis, *AIAA J.* **14** (1976) 705.
[8] P. J. Lamont and B. L. Hunt, *J. Fluid Mechanics* **100** (1977) 471.
[9] M. D. Desphande and R. N. Vaishnav, *ibid.* **114** (1982) 213.
[10] E. Loth and G. M. Faeth, *Int. J. Multiphase Flow* **15** (1989) 589.
[11] J. Stevens and B. W. Webb, *Int. J. Heat Mass Transf.* **36** (1993) 3751.
[12] D. Cooper, D. C. Jackson, B. e. Launder and G.X. Liao, *ibid.* **36** (1993) 2675.
[13] A. S. Mjumdar and W.J.M. Douglas, 'Impingement Heat Transfer: A Literature Survey', Tappi Meeting, 3 Oct. (1973), New Orleans.
[14] K. Jambunatham, E. Lai, M. A. Moss and B. L. Button, *Int. J. Heat and Fluid Flow* **13** (1992) 106.
[15] K. Kataoka and T. Mizushina, Proceedings of 5th International Heat Transfer Conference, Tokyo (1974) 305.
[16] M. A. Patrick, D. J. Tagg, E. A. Vallis and A. A. Wragg, AIChE Meeting, Nov. (1977), New York.
[17] E. A. Vallis, M. A. Patrick and A. A. Wragg, Proceedings of Euromech. 90, Nancy, France, July (1977).
[18] *Idem*, Proceedings of International Heat Transfer Conference, Toronto, Sept. (1978).
[19] D-T. Chin and C-H. Tsang, *J. Electrochem. Soc.: Electrochem. Sci. and Technol.* **125** (1978) 1461.
[20] R. C. Alkire and T-J. Chen, *ibid.* **129** (1982) 2424.
[21] A. A. Sonin, *ibid.* **130** (1978) 1501.
[22] J. Nanzer, A. Donizeau and F. Coeuret, *J. Appl. Electrochem.* **14** (1984) 51.
[23] T. Mizushina, *Adv. Heat Transf.* **7** (1971) 87.
[24] A. A. Wragg, *The Chemical Engineer* No. 316 (1977) 39.
[25] J. R. Bourne and P. Dell'Ava, O. Dossenbach and T. Post, *J. Chem. Eng. Data* **30** (1985) 160.
[26] F. P. Berger and A. Ziai, *Ind. Chem. Eng. Res. Des.* **61** (1983) 377.
[27] T. J. Hanratty, 'Heat and Mass Transfer in Boundary Layers' edited by N. Afgan, Z. Zaric and P. Anastasijevic (Pergamon Pres, New York, 1972), p. 919.
[28] E. Achenbach, *Int. J. Heat Mass Transf.* **18** (1975) 1387
[29] Q. Li and J.D.A. Walker, *AIChE J.* **42** (1996) 391.
[30] V. V. Rao and O. Trass, *Can. J. Chem. Eng.* **42** (1964) 95.